

# RSC Advances



This is an *Accepted Manuscript*, which has been through the Royal Society of Chemistry peer review process and has been accepted for publication.

*Accepted Manuscripts* are published online shortly after acceptance, before technical editing, formatting and proof reading. Using this free service, authors can make their results available to the community, in citable form, before we publish the edited article. This *Accepted Manuscript* will be replaced by the edited, formatted and paginated article as soon as this is available.

You can find more information about *Accepted Manuscripts* in the [Information for Authors](#).

Please note that technical editing may introduce minor changes to the text and/or graphics, which may alter content. The journal's standard [Terms & Conditions](#) and the [Ethical guidelines](#) still apply. In no event shall the Royal Society of Chemistry be held responsible for any errors or omissions in this *Accepted Manuscript* or any consequences arising from the use of any information it contains.

## In-situ electron beam irradiation-driven formation of quantum Dots

Haibo Zeng,<sup>a,b,c</sup>\* Xiaoming Li,<sup>a,b</sup> Huijie Zhao,<sup>a,b</sup> Xue Ning<sup>a,b</sup>, Jiayue Xu<sup>c</sup>

<sup>a</sup>State Key Laboratory of Mechanics and Control of Mechanical Structures & College of Materials Science and Technology, Nanjing University of Aeronautics and Astronautics, Nanjing 210016, China

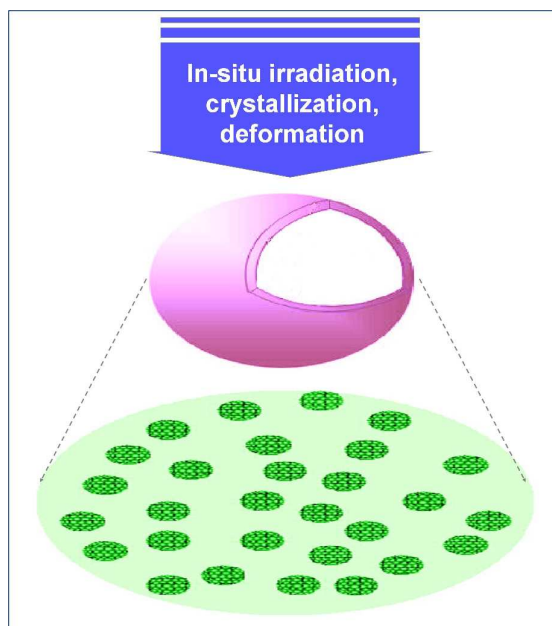
<sup>b</sup>Institute of Optoelectronics & Nanomaterials, College of Materials Science and Engineering, Nanjing University of Science and Technology, Nanjing 210094, China

<sup>c</sup>Institute of Crystal Growth, School of Materials Science and Engineering, Shanghai Institute of Technology, Shanghai 201418, P.R. China

\*Correspondence and requests for materials should be addressed to H.B.Z. ([zeng.haibo@njust.edu.cn](mailto:zeng.haibo@njust.edu.cn))

**Abstract** Recrystallization of amorphous materials is a very interesting phenomenon, but still unknown in some transformation details. Here, we report on the formation of ZnO quantum dots (QDs) under electron beam irradiation and a series of *in-situ* consecutive observations on the formation processes. When suffering from the irradiation inside a transmission electron microscope (TEM), the amorphous hollow nanoparticles, fabricated through treating the Zn/ZnO core-shell samples synthesized by laser ablation in liquid with tartaric acid, were found to gradually collapse, and the crystallization occurred at the same time. These two isochronous processes collectively induced the formation of the QDs. Interestingly, the size of QDs can be controlled by the applied precursor particles and beam energy. The numerical simulations demonstrated that the thermal shear stresses greatly stimulate the deformation process, resulting in QDs formation.

### TOC Picture



## 1. Introduction

Recrystallization of amorphous materials is a very interesting phenomenon, but still unknown in some transformation details. The instability of materials when their dimensions come into the nanoscale becomes a significant issue both for fundamental understanding of nanomaterials and for their applications.<sup>1,2</sup> For example, large thermal instability was reported to induce great changes in electrical conductance of Ga-doped ZnO.<sup>3</sup> During an electrocatalysis process, the supported Pt nanoparticle catalysts could also exhibit strong instability in size, shape, and microstructure. This greatly degrades the performance of a fuel cell.<sup>4</sup> During the chemical vapor deposition growth of Si nanowires, the instability of metal catalyst nanoparticles was reported to largely affect a vapor-liquid-solid process. This could be used to control the product morphology.<sup>5</sup> Li et al. pointed out that the instability could be caused by a combined effect of structural disorder and inhomogeneous strain fields.<sup>6</sup> Joshi et al. demonstrated that a grain rotation contributes much to the shear instability of nanocrystalline and amorphous materials, and is size-dependent.<sup>7</sup> However, it is noted that both theoretical and experimental works which treat the regarded instabilities have been very few to date.

On the other hand, amorphous hollow nanoparticles provide the idea model materials for the investigation of recrystallization of amorphous materials with in-situ observation inside TEM. Hollow nanostructures have attracted an increasing interest because of their specific morphologies and properties that differ from bulky counterparts,<sup>8-15</sup> and hence have prominent applications in drug-delivery,<sup>16,17</sup> catalysis,<sup>18,19</sup> and biologic imaging.<sup>20,21</sup> However, due to peculiar structural features, such as hollow interiors and thin shells, they could behave differently with respect to instability. The confirmations of such behavior however have been lacking till now due to numerous experimental difficulties. Fan et al. observed mass diffusion along the inner pore surfaces in the hollow nanostructures.<sup>22,23</sup> Previously, we documented a structural instability of

amorphous ZnO hollow nanoparticles (HNPs) during a photocatalysis process. Such instability can be hindered by the intercalation of ultrafine noble metal nanoparticles (NPs) and by improving the ZnO matrix crystallinity.<sup>18</sup> On the other hand, recently, *in-situ* processes and synchronous observations inside a transmission electron microscopy (TEM) have become a very cogent way for the structural and property investigations of nanostructures. This technique endows a researcher a “hand” (*in-situ* nanomanipulation) and an “eye” (*in-situ* imaging) at the same time.<sup>24-28</sup> Therefore, the *in-situ* TEM could provide an effective way for a study of crystallization and instability of NPs.

Herein, we present *in-situ* TEM investigations of crystallization and deformation of ZnO HNPs under focused electron beam irradiation. Pronounced instability, manifested by dramatic deformations, was observed during crystallization. This induced a collapse of HNPs and their transformation into monodispersed ZnO quantum dots (QDs) with loose substrate limitation, possibly precise locating, and facile size control. The features and processes of deformations were subtly observed, and then the simulated shear stresses within HNPs were thoroughly analyzed. These results would be particularly important for the understanding of small nanostructures grown by a solution method,<sup>1,2,18</sup> and could be utilized for diverse nanofabrications.

## 2. Experiments

**Formation of Zn-ZnO core-shell nanoparticles.** The ZnO amorphous HNPs were synthesized by laser ablation in liquid and subsequent weak acid etching. Firstly, a zinc plate (99.99%) was fixed on a bracket in a glass vessel filled with 10 ml 0.05 M sodium dodecyl sulfate (99.5%) aqueous solution. The plate was ablated (irradiated) for 30 min by the first harmonic of Nd: YAG laser (1064 nm, frequency 10 Hz, pulse duration 10 ns) with a 2 mm focused spot.

**Formation of amorphous ZnO hollow nanoparticles.** After the formation of nanoparticle by laser ablation in liquid, the 50 ml obtained colloidal solutions were etched by tartaric acid (TA,  $C_4H_6O_6$ , 10 mM, 20 ml). The etching agents were slowly dropped into the colloidal solution, droplet by droplet, at the invariable temperature 40 °C on a stirrer with a heating pedestal. After etching, the colloidal solutions were centrifuged at 14000 rpm and then ultrasonically re-dispersed in ethanol for more than five cycles to remove the surfactants, and finally draught-dried in an oven at 40 °C for 24 h.

**In-situ observation on the formation of ZnO quantum dots.** The in-situ electron beam irradiation experiments were carried out in a high resolution transmission electron microscope (HRTEM, JEOL JEM 2010F) operated at 200 kV. The nanoparticles were re-dispersed in pure ethanol and collected on a TEM copper grid covered with an amorphous carbon film for electron irradiation and HRTEM observations.

### 3. Results and discussion

The starting materials, the ZnO HNPs, were fabricated by laser ablation and subsequent weak acid-etching as discussed in our previous reports.<sup>18,29,30,31</sup> The diameters of HNPs could be adjusted from 10 to 50 nm under a fabrication process. The small HNPs had an amorphous structure, but the larger HNPs exhibited few crystalline ultrafine grains, which are surrounded by disordered areas within the shells.<sup>18,31</sup> The *in-situ* electron beam irradiation was carried out in a HRTEM on HNPs dispersed on carbon-coated grids.

**3.1. Process of in-situ crystallization and deformation.** The consecutive morphological evolutions of a single ZnO HNP under the electron irradiation were recorded by a series of HRTEM images, as shown in Fig. 1. The primal HNP has a diameter of 12 nm and an intact spherical appearance (Fig. 1 (a)). After flash irradiation, notable structural distortion takes place, especially at the particle surface, Fig. 1 (b). Such deformation becomes more profound with an irradiation time increasing, as seen in Fig. 1 (b) to (c). At the

same time, the mass aggregation occurs in Fig. 1 (c), as reflected by the appearance of small dots of a dark contrast. With further irradiation, the mass aggregation becomes more apparent and the discrete new dots become clearly visible, Fig. 1 (d). The hollow shell matrix is still preserved. The subsequent irradiation leads to a final collapse of HNP. The process is accompanied with the appearance of many ultrafine particles, as presented in Fig. 1 (e) (30 s irradiation). The additional irradiation promotes the particle separation [Fig. 1 (f), (g), and (h)].

The changes of crystallinity and composition before and after electron irradiation were then analyzed. The selected area electron diffraction (SAED) pattern of a starting HNP in Fig. 1 (a) exhibits faint halos (Fig. 2 (a)), indicating an amorphous state, which is in accord with our previous report.<sup>18</sup> After irradiation, (Fig. 1 (h)), the SAED pattern taken from the same area exhibits many bright diffraction spots. These form incomplete diffraction rings which can be indexed to a wurtzite ZnO in Fig. 2 (b). On the other hand, from the EDS spectra in Fig. 2 (c), the Zn/O ratios before and after irradiation are 0.91:1 and 0.88:1, respectively, thus close to the stoichiometric compositions. It is noted that previously, Du et al. reported the crystallization of amorphous SiO<sub>2</sub> by ex-situ electron beam irradiation and a product was found to be crystalline Si.<sup>32</sup> By contrast, Andrew et al. reported that Fe oxide compositions were preserved during irradiation-induced crystallization of amorphous Fe oxide NPs.<sup>33</sup> Our data shows that the Zn oxide reduction does not take place in the present case as well.

We assume here that the above irradiation-driven evolution may actually contain two underlying processes of *in-situ* crystallization and synchronous HNP deformation leading to monodispersed ZnO QD formation.

An edge area of an HNP was particularly analyzed in Fig. 3. The disordered state is obvious for the starting HNP, as shown in Fig. 3 (a). After short-time irradiation, two grains denoted as “A” and “B” in Fig.

3 (b) appeared. During irradiation, they are flickering in the field of view and act as embryo nucleus. At the same time, the contrast of the grains' surrounding area gradually fades away, which indicates the atomic migration towards the grains. This feeds the grain growth. Under further atomic migrations new grains appear and the former grains grow. On the other hand, such migration towards the grains forms spatial gaps among them, leading to a marked separation, as shown in Fig. 3 (c). Moreover, the grain diffusion (described below) should also contribute to the regarded morphology changes.

**3.2. Process features: volume expansion and size effect.** From the *in-situ* TEM observations, it is apparent that the crystallization and deformation has two peculiar features, namely, volume expansion and size effect. The former is well reflected by Fig. 1, where the dashed circles point out the primal HNP's areas. Under the electron irradiation, the HNP gradually expands, from Fig. 1 (a) to (b), (c), and (d). Typically in Fig. 1 (d), the primal area becomes notably smaller (after 20 s irradiation) compared to the initial state. The corresponding radius and volume increase to ~15% and ~55%, respectively. Considering the preserved integrality of HNP and a so high expansion ratio, it is believed that the process does not reflect a conventional thermal expansion. The collapse of HNP may thus be regarded as a result of volume expansion under internal stresses. When such stress exceeds a critical value, a ZnO HNP collapses due to its high brittleness and low cohesive energy.

On the other hand, the process exhibits significant size effects, as shown in Fig. 4. The size of starting HNPs is 30, 20, and 12 nm (Fig. 4 (a), (b), and (c)), whereas the average diameters of obtained QDs after electron irradiation are 3.4, 2.5, and 1.2 nm (Fig. 4 (d), (e), and (f)), respectively. The lattice fringes corresponding to the ZnO (002) planes are visible. The QDs have a narrow size distribution. Noticeably, the sizes of these QDs are comparable with the Bohr diameter of ZnO (1.8 nm). Therefore, the pronounced quantum effects and corresponding changes in optical properties could be envisaged in line with the

effective-mass approximation model.<sup>34</sup> Compared with the conventional fabrication routes of QDs,<sup>35,36</sup> the reported process has several sound advantages. They are namely: (i) no particular demands to a substrate; (ii) precise QDs positioning (the starting HNP could be pre-located), and (iii) a facile size control. These features make the *in-situ* process and the resultant QDs highly useful for the optical and optoelectronic nanodevice applications.

Thermodynamically, the *in-situ* crystallization of ZnO HNPs was stimulated by a thermal effect of electron beam irradiation, which is similar to amorphous SiO<sub>2</sub><sup>32</sup> and Fe oxide<sup>33</sup> cases. The irradiation with  $\sim 2 \times 10^6$  e/s nm<sup>2</sup> intensity could rapidly induce the temperature rise in the materials. The highest temperature for the present ZnO HNPs is estimated to be in the range of 400 to 600 K.<sup>37</sup> On the other hand, electron beam heating is reported to decrease the nucleation barrier, which also promotes crystallization.<sup>32</sup>

The observed HNPs deformation under irradiation needs a special attention. Although the volume expansion was observed during the amorphous-crystallization of a metal-glasses due to an increase in “free volume”, the expansion rate documented herein is much larger than those reported for any metal glass.<sup>38</sup> The huge volume expansion of ZnO HNPs could be taken as a macroscopical response to the atomic migrations and grains' separations.<sup>6</sup> For example, the grain (B) is obviously away from its original position in Fig. 3 (c). The outward direction is dominant for the observed volume expansion and deformation. This indicates that the large thermal shear stresses could exist within the HNPs shells.

**3.3. Simulated shear stress and its size effect.** Fig. 5 (a) presents the 3-dimensional and planar structural models for ZnO HNPs, where  $r_{in}$ ,  $r_{out}$  and  $r$  are the the inner, outer radii, and a distance to a given mass within the shell, respectively. The applied structural parameters of HNPs are indexed as  $(r_{in}, r_{out})$ . We focus on a site-dependent shear stress, and set the boundary conditions as following:  $r = r_{in}$ ,  $\sigma = 0$  and  $r = r_{out}$ ,  $\sigma = 0$ , where  $\sigma$  is a thermal stress in the radial direction. According to the thermal elastic theory,<sup>39,40,41</sup> the radial

and tangential stresses based on spherical coordination ( $d\theta = d\varphi, \sigma_\theta = \sigma_\varphi$ ) under the equilibrium conditions could be expressed as:

$$\frac{d\sigma_r}{dr} + \frac{1}{r}(2\sigma_r - \sigma_\theta - \sigma_\varphi) = 0, \quad r_{in} \leq r \leq r_{out} \quad (1)$$

In the case of external temperature approach, the total thermal strain is written as:

$$\varepsilon_r - \alpha T = \frac{1}{E}(\sigma_r - 2\nu\sigma_\theta) \quad \text{and} \quad \varepsilon_\theta - \alpha T = \frac{1}{E}[(1-\nu)\sigma_\theta - \nu\sigma_r] \quad (2)$$

where  $T$  is a function of the shell thickness, and satisfies:  $\frac{d}{dr}\left(r \frac{dT}{dr}\right) = 0$  within a spherical shell. Therefore,

the stress in the radial direction is deduced as:

$$\sigma_r = \frac{2\alpha E}{1-\nu} \left[ \frac{r^3 - a^3}{b^3 - a^3} \frac{1}{r^3} \int_a^b Tr^2 dr - \frac{1}{r^3} \int_a^r Tr^2 dr \right] \quad (3)$$

Then, a site-dependent thermal shear stress can be simulated as illustrated in Fig. 5 (b) according to different structural configurations, and then the stress gradients (Fig. 5 (c)) can be obtained from the site-dependent stresses. In case of HNPs, the large shear stresses can be induced by electron beam heating. The maximum stresses in the shells are as high as 6~30 MPa, which means that the activation energy up to 0.01 eV should be taken into account. This may excite the regarded atomic migrations and grains' diffusion under crystallization and deformation processes. More importantly, the stress gradients can be as high as 6~28 MPa in Fig. 5 (c), which could induce inhomogeneity of structure response to electron beam heating. This well support the morphological evolutions of HNPs observed in Fig. 1 and Fig. 3. Similarly, Spaepen demonstrated that small thermal fluctuations could break any existing defect in an amorphous metal into small segments with lower configuration energies.<sup>42</sup>

For the HNPs with different structural configurations, shear stresses exhibit obvious size effects. Through comparing the curves in Fig. 5 (b), one can see that the shear stress intensity decreases with an increase in  $r_{in}$  and  $r_{out}$ . For example, the stress decreases from 29.4 to 8.8 MPa with radius increasing from 6 to 14 nm. The stress gradients also decrease from 27.4 to 5.6 MPa/nm with an original HNP size enlarging. The

decreased intensity and gradient of a shear stress would depress the activity of atomic migration and grain diffusion. Such changes in the larger HNPs would make the deformation process milder during crystallization, and advance the grains to grow larger in the thermodynamically conditions with higher equilibrium. This is in accord with a size decrease of resulted QDs from the smaller starting HNPs, as observed in Fig. 4. Previously, Joshi and Ramesh theoretically treated the size effects of a grain rotation, which induced the shear instability in the nanocrystalline and amorphous materials.<sup>7</sup>

Furthermore, it is worth noting that the size effects of shear stresses and their gradients are much more significant for the small size range. With the size decreasing, the increasing rates of the intensity and the gradient of a shear stress become abrupt (i.e. when a radius is below 20 nm in Fig. 5 (b) and (c)). By contrast, these rates are nearly saturated and only marginally changeable in the large size range. These phenomena demonstrate that the instability will become more dominant in the smaller HNPs where the stronger deformation should occur during the crystallization. Li's simulations also showed that a disorder and internal inhomogeneous strain fields play an important role in the instability.<sup>6</sup> Recently, we have also observed the significant enhancement of instability of ZnO and ZnS nanowires when the concentration of dopants was in a certain range, that also induces the local disorder and stress-strain fields within a lattice.<sup>43</sup>

#### 4. Conclusions

In summary, the *in-situ* HRTEM observations have been performed to explore the crystallization and deformation of ZnO HNPs under focused electron beam irradiation. A series of violent morphological changes were observed. These resulted in HNPs collapse and their transformation into monodispersed ZnO QDs. Compared with the conventional routes, the present QDs formation process has several sound advantages such as no specific requirements for a substrate, precise QDs location and size control. The

detailed observations demonstrate that the atomic migration and grains' separation are the kinematic inducements of the dramatic HNPs deformations under crystallization, accompanied with the huge HNPs volume expansions and notable size effects. The numerical simulations demonstrate that the thermal shear stresses and their gradients greatly stimulate the atomic migrations and grains' diffusions, and hence the dramatic deformations. The size effects of the calculated thermal shear stresses presume their dominance for the small-sized HNPs and for those exhibiting an amorphous or partially disordered state. These would induce larger deformations during a crystallization process and could be utilized for the smart QDs nanofabrication.

### Acknowledgements

This work was supported by the National 973 project from National Basic Research Program of China (2014CB931700/2014CB931702) and the National Natural Science Foundation of China (61222403). A Project Funded by the Priority Academic Program Development of Jiangsu Higher Education Institutions.

### References

- 1 M. Li and W. L. Johnson, *Phys. Rev. Lett.*, 1993, **70**, 1120.
- 2 X. M. Bai and M. Li, *Nano Lett.*, 2006, **6**, 2284.
- 3 J. A. Sans, G. M. Criado, J. P. Porres, J. F. S. Royo and A. Segura, *Appl. Phys. Lett.*, 2007, **91**, 221904.
- 4 Y. S. Shao-Horn, C. Sheng, W. S. Chen, P. J. Ferreira and D. Morgan, *Top Catal.*, 2007, **46**, 285.
- 5 L. Cao, B. Garipcan, J. S. Atchison, C. Ni and J. E. Spanier, *Nano Lett.*, 2006, **6**, 1852.
- 6 G. P. Zheng and M. Li, *Acta. Mater.*, 2007, **55**, 5464.
- 7 S. P. Joshi and K. T. Ramesh, *Phys. Rev. Lett.*, 2008, **101**, 025501.
- 8 Y. D. Yin, R. M. Rioux, C. K. Erdonmez, S. Hughes and A. P. Alivisatos, *Science*, 2004, **304**, 711.
- 9 P. X. Gao and Z. L. Wang, *J. Am. Chem. Soc.*, 2003, **125**, 11299.
- 10 M. S. Mo, J. C. Yu, L. Z. Zhang and S. K. A. Li, *Adv. Mater.*, 2005, **17**, 756.

- 11 M. S. Mo, S. H. Lim, Y. W. Mai, R. K. Zheng and S. P. Ringer, *Adv. Mater.*, 2008, **20**, 339.
- 12 F. Q. Sun and J. C. Yu, *Angew. Chem. Int. Ed.*, 2007, **46**, 773.
- 13 G. Z. Shen, Y. Bando, C. H. Ye, X. L. Yuan, T. Sekiguchi and D. Golberg, *Angew. Chem. Int. Ed.*, 2006, **45**, 7568.
- 14 K. An, S. G. Kwon, M. Park, H. B. Na, S. Baik, J. H. Yu, D. Kim, J. S. Son, Y. W. Kim and H. M. Park, T. Hyeon, *Nano Lett.*, 2008, **12**, 4252.
- 15 H. J. Fan, U. Gösele and M. Zacharias, *Small*, 2007, **3**, 1660.
- 16 E. Mathiowitz, J. S. Jacob, Y. S. Jong, C. A. Santos, K. Vijayaraghavan, S. Montgomery, M. Bassett and C. Morrell, *Nature*, 1997, **386**, 410.
- 17 T. Yamada, Y. Iwasaki, H. Tada, H. Iwabuki, M. K. L. Chuah, T. VandenDriessche, H. Fukuda, A. Kondo and M. Ueda, M. Seno, *Nat. Biotechnol.*, 2003, **21(8)**, 885.
- 18 H. B. Zeng, W. P. Cai, P. S. Liu, X. X. Xu, H. J. Zhou, C. Klingshirn and H. Kalt, *ACS Nano*, 2008, **2**, 1661.
- 19 B. X. Li, Y. Xie, M. Jing, G. X. Jing, G. X. Rong, Y. C. Tang and G. Z. Zhang, *Langmuir*. 2006, **22**, 9380.
- 20 C. H. Su, H. S. Sheu, C. Y. Lin, C. C. Huang, Y. W. Lo, Y. C. Pu, J. C. Weng, D. B. Shieh, J. H. Chen and C. S. Yeh, *J. Am. Chem. Soc.*, 2007, **129**, 2139.
- 21 J. Chen, F. Saeki, B. J. Wiley, H. Cang, M. J. Cobb, Z. Y. Li, L. Au, H. Zhang, M. B. Kimmey, X. Nan and D. Li, *Nano. Lett.*, 2005, **5**, 473.
- 22 H. J. Fan, M. Knez, R. Scholz, D. Hesse, M. Zacharias and U. Gösele, *Nat. Mater.*, 2006, **5**, 627.
- 23 H. J. Fan, M. Knez, R. Scholz, D. Hesse, K. Nielsch, M. Zacharias and U. Gösele, *Nano. Lett.*, 2007, **7**, 993.
- 24 D. Golberg, P. M. F. J. Costa, M. Mitome and Y. Bando, *J. Mater. Chem.*, 2009, **19**, 909.
- 25 Y. Gao and Y. Bando, *Nature*, 2002, **415**, 599.
- 26 H. G. Duan, E. Q. Xie, L. Han and Z. Xu, *Adv. Mater.*, 2008, **20**, 3284.
- 27 Y. J. Gan and F. Banhart, *Adv. Mater.*, 2008, **20**, 4751.
- 28 Y. Yang, R. Scholz, A. Berger, D. S. Kim, M. Knez, D. Hesse, U. Gösele and M. Zacharias, *Small*, 2008, **4**, 2112.
- 29 H. B. Zeng, W. P. Cai, Y. Li, J. L. Hu and P. S. Liu, *J. Phys. Chem. B*, 2005, **109**, 18260.
- 30 H. B. Zeng, Z. G. Li, W. P. Cai, B. Q. Cao, P. S. Liu and S. K. Yang, *J. Phys. Chem. B*, 2007, **111**, 14311.
- 31 Zeng, H. B., Liu, P. S., Cai, W. P., Yang, S. K. and Xu, X. X., *J. Phys. Chem. C*, 2008, **112**, 19620.
- 32 X. W. Du, M. Takeguchi, M. Tanaka and K. Furuya, *Appl. Phys. Lett.*, 2003, **82**, 1108.
- 33 A. H. Latham, M. J. Wilson, P. Schiffer and M. E. Williams, *J. Am. Chem. Soc.*, 2006, **128**, 12632.
- 34 Y. Kayanuma and *Phys. Rev. B*, 1988, **38**, 9797.
- 35 Y. S. Fu, X. W. Du, S. A. Kulinich, J. S. Qiu, W. J. Qin, R. Li and J. Liu, *J. Am. Chem. Soc.*, 2007, **129**, 16029.

- 36 J. G. Lu, Z. Z. Ye, Y. Z. Zhang, Q. L. Liang, Sz. Fujita and Z. L. Wang, *Appl. Phys. Lett.*, 2006, **89**, 023122.
- 37 M. Liu, L. Y. Xu and X. Z. Lin, *Scanning*, 1994, **16**, 1.
- 38 Q. K. Li and M. Li, *Phys. Rev. B*, 2007, **75**, 094101.
- 39 G. Ouyang, X. L. Li and G. W. Yang, *Appl. Phys. Lett.*, 2007, **91**, 051901.
- 40 G. Ouyang, X. L. Li, X. Tan and G. W. Yang, *Phys. Rev. B*, 2007, **76**, 193406.
- 41 C. Q. Sun, *Prog. Solid State Chem.*, 2007, **35**, 1.
- 42 F. Spaepen, *Defects in Amorphous Solids*, Les Houches Lectures on Physics of Defects (North-Holland, Amsterdam, **1981**), pp. 133-174.
- 43 B. Liu, Y. Bando, X. Jiang, C. Li, X. Fang, H. B. Zeng, T. Terao, C. Tang, M. Mitome, D. Golberg, *Nanotech.*, 2010, **21**, 375601.

### Figure captions

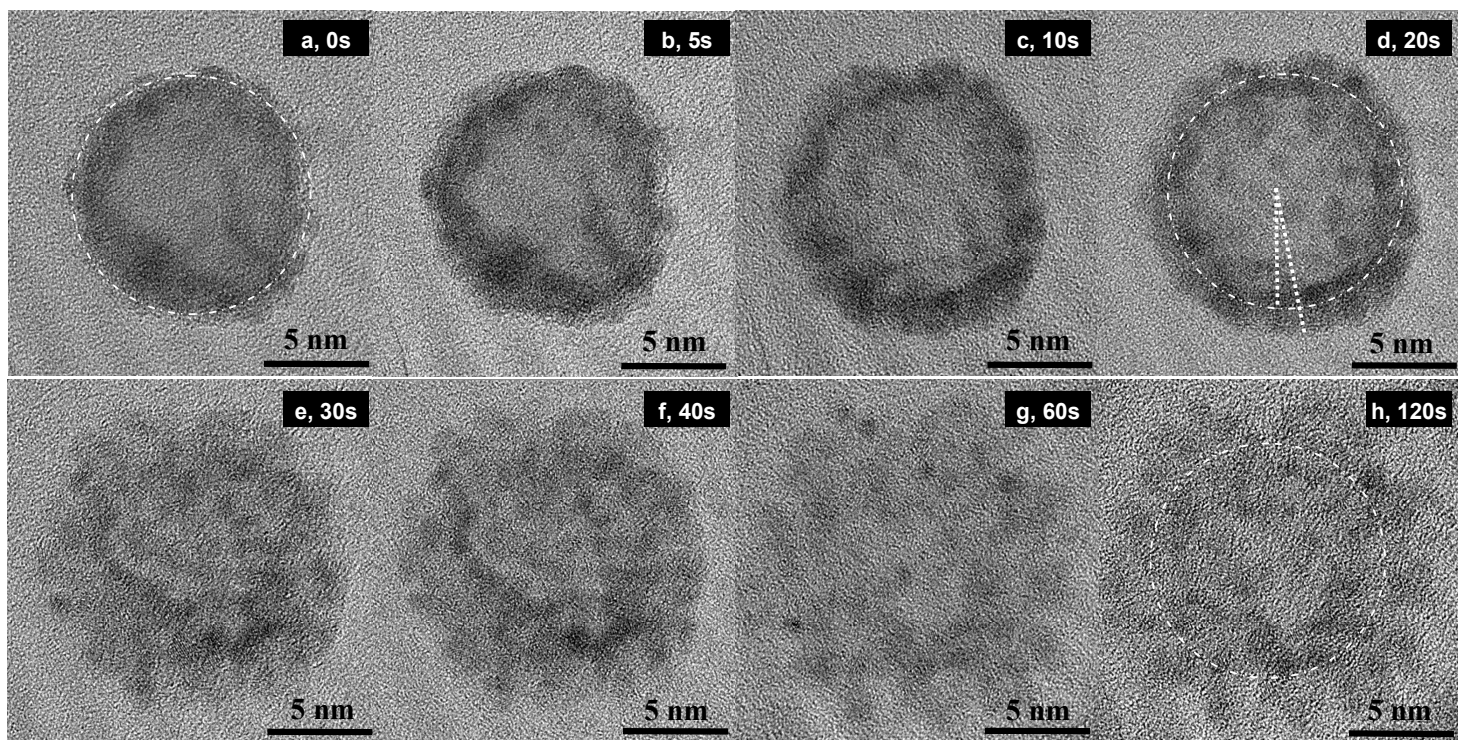
Fig. 1 In-situ HRTEM irradiation and imaging of consecutive evolutions of an individual ZnO HNP under irradiation with a focused electron beam. The dashed circles index the area of the starting HNPs.

Fig. 2 Comparison of SAED patterns before (a) and after (b) electron irradiation, and the corresponding EDS spectra (c).

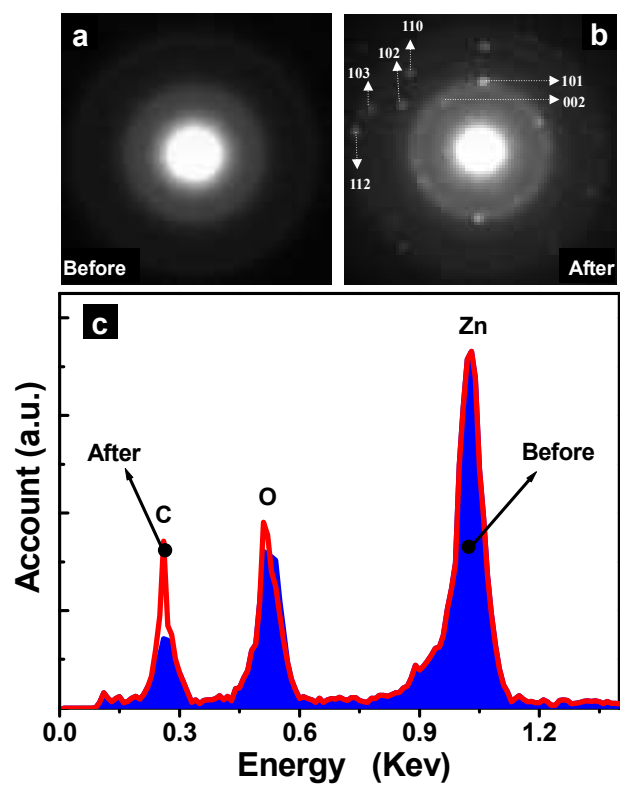
Fig. 3 Local HRTEM observations of the HNP edge area evolutions under 0 s (a), 10 s (b), and 20 s (c) electron irradiations. The dashed circles point out the nascent and grown grains.

Fig. 4 HRTEM images of selected single HNPs with diameter of 30 (a), 20 (b), and 12 (c) nm, and the correspondingly transformed QDs (d), e, and f, respectively.

Fig. 5 Structural models of HNPs (a), numerically simulated site-dependent thermal shear stresses (b), and diameter-dependent gradients (c). Here,  $r_{in}$ ,  $r_{out}$ , and  $r$  are the inner, outer radii, and a distance to a given mass site within the shell. The applied structural parameters of HNPs are indexed as ( $r_{in}$ ,  $r_{out}$ ).



**Fig. 1** *In-situ* HRTEM irradiation and imaging of consecutive evolutions of an individual ZnO HNP under irradiation with a focused electron beam. The dashed circles index the area of the starting HNPs.



**Fig. 2** Comparison of SAED patterns before (a) and after (b) electron irradiation, and the corresponding EDS spectra (c).

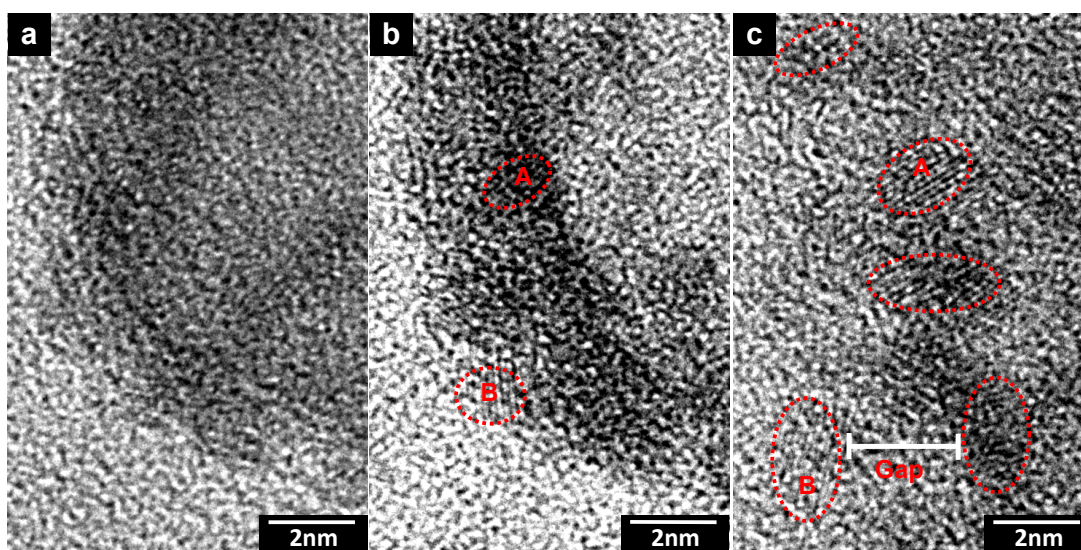


**Fig. 3** Local HRTEM observations of the HNP edge area evolutions under 0 s (a), 10 s (b), and 20 s (c) electron irradiations. The dashed circles point out the nascent and grown grains.

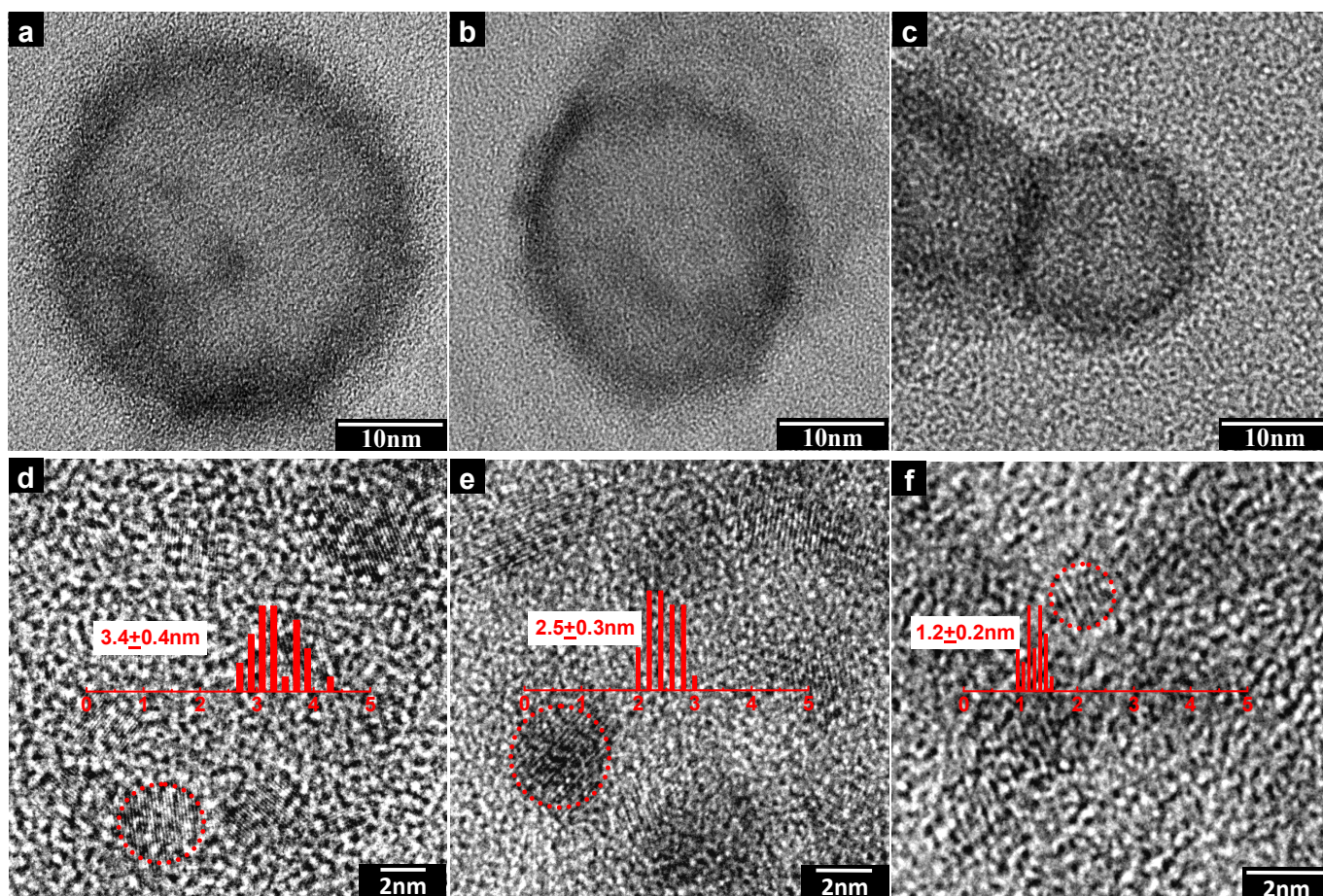


**Fig. 4** HRTEM images of selected single HNPs with diameter of 30 (a), 20 (b), and 12 (c) nm, and the correspondingly transformed QDs (d), e, and f, respectively.

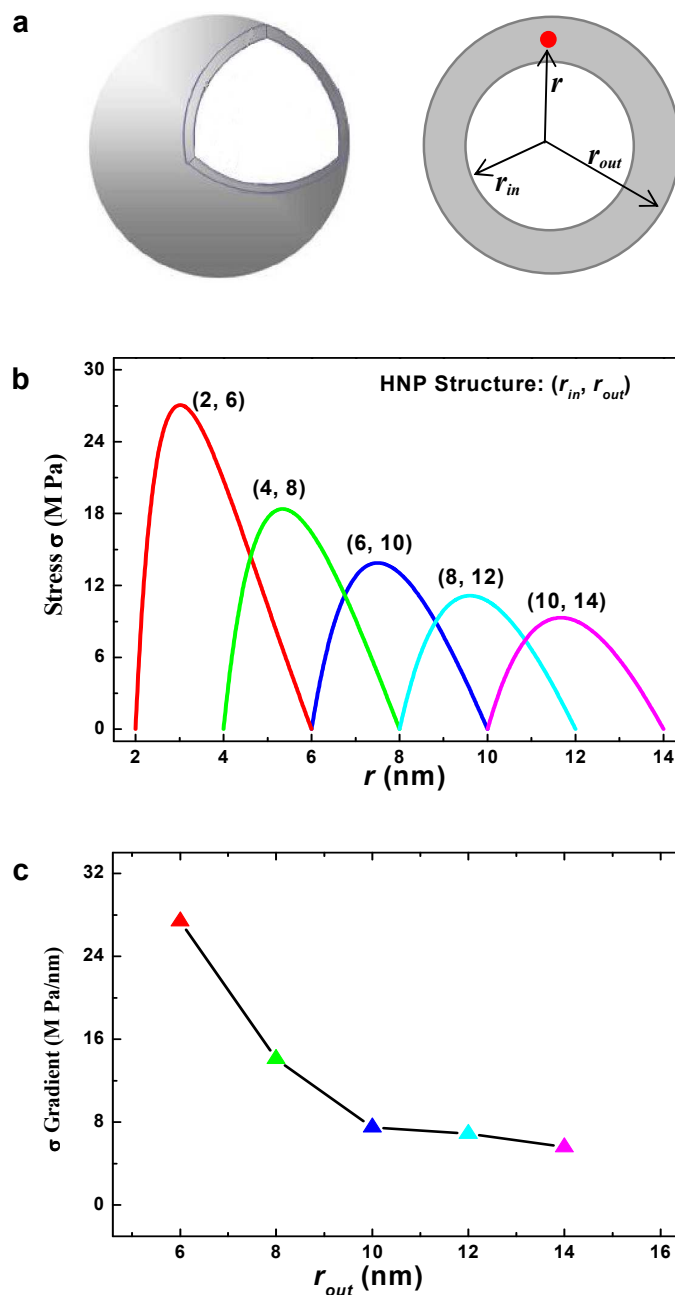


**Fig. 5** Structural models of HNPs (a), numerically simulated site-dependent thermal shear stresses (b), and diameter-dependent gradients (c). Here,  $r_{in}$ ,  $r_{out}$  and  $r$  are the inner, outer radii, and a distance to a given mass site within the shell. The applied structural parameters of HNPs are indexed as  $(r_{in}, r_{out})$ .